

# Optical parametric amplification of a supercontinuum in a gas

Yuichiro Kida · Totaro Imasaka

Received: 14 September 2013 / Accepted: 11 December 2013 / Published online: 20 December 2013  
© Springer-Verlag Berlin Heidelberg 2013

**Abstract** Amplification of supercontinuum light via four-wave optical parametric amplification in a gas-filled hollow fiber is investigated. By pumping with a femtosecond pulse in the near-infrared, amplification was observed in the wavelength range 500–700 nm, with an amplification gain up to 100. The amplification bandwidth obtained here supports sub-10-fs pulse durations. The wavelength and gas-pressure dependence of the amplification gain in this regime significantly differ from those predicted from only the linear phase mismatch. The nonlinear phase mismatch, arising from nonlinear phase modulations induced by a pump pulse, dominates the features observed for the amplification, i.e., a low phase-matching pressure and an amplification gain depending on wavelength. To investigate the effect of phase modulations on the parametric amplification, numerical analysis and simulations are used to reproduce the measured wavelength dependence of the amplification gain.

## 1 Introduction

Light amplification by optical parametric amplification (OPA) in birefringent crystals has been investigated with regard to generating ultrashort visible and near-infrared pulses [1, 2]. In addition, high peak powers achievable with

chirped input pulses provide means to develop a laser system delivering sub-10-fs pulses with PW-scale peak power [3]. Until now, generation of sub-10-fs pulses with multi-TW peak powers has been reported [4, 5] and applied in the generation of monoenergetic electron bunches via relativistic light–matter interaction [6]. Recently, the use of high-power picosecond or sub-picosecond laser pulses from a thin-disk laser or an Innoslab laser has been evaluated for optical parametric chirped-pulse amplification (OPCPA) [7, 8]. Because a supercontinuum for seeding an OPCPA is also available by focusing such picosecond or sub-picosecond pulses into a bulk medium, Ti:sapphire-free OPCPA can be developed resulting in a compact setup [8–10] that potentially could yield high-stability. One of the potential issues in this Ti:sapphire-free OPCPA scheme is that the typical pulse energy obtained for the supercontinuum is low (in the nJ range at most), requiring a notably high gain in the OPCPA when amplifying up to TW–PW peak powers. Generation of parametric fluorescence in the OPCPA might not be negligible, thereby degrading the phase and energy stabilities as well as the temporal contrast of the amplified pulses [11].

In this instance, a preamplifier amplifying the energy of a supercontinuum by 2–3 orders of magnitude is useful. The gain required in the main OPCPA stage then decreases by the same order, reducing the intensity of the parametric fluorescence generated in the OPCPA stage to a negligible level. Four-wave optical parametric amplification (FWOPA) [12–16] is a candidate for the preamplification process. Amplification gains as high as 80 and 100 in a fused silica and water, respectively, have been reported together with a broad amplification wavelength range supporting sub-10-fs pulse durations [12, 15]. Broader amplification bandwidth can be realized using a gas medium in the FWOPA because of the lower group-velocity

Y. Kida (✉) · T. Imasaka  
Department of Applied Chemistry, Graduate School of  
Engineering, Kyushu University, 744 Motoooka, Nishi-ku,  
Fukuoka 819-0395, Japan  
e-mail: y-kida@cstf.kyushu-u.ac.jp

T. Imasaka  
Division of Optoelectronics and Photonics, Kyushu University,  
744 Motoooka, Nishi-ku, Fukuoka 819-0395, Japan

dispersion (GVD) in the medium than the bulk media. Four-wave mixing (FWM) in a gas has been investigated for frequency conversion [17–21]. There is also a report regarding light amplification using narrowband input pulses and high-order propagation modes [22]. Direct amplification of a broadband input pulse in a gas has not been studied in regard to the wavelength dependence of the amplification gain and the effect of nonlinear phase modulations on amplification.

In this report, our investigation of FWOPA in a gas-filled hollow fiber seeded with a supercontinuum pulse is described. The aim was to clarify the wavelength dependence of the amplification gain and the effect of nonlinear phase modulations on amplification gain. In contrast to a previous work [22], the fundamental propagation mode  $\text{EH}_{11}$  is used for all pump, signal, and idler pulses. This regime of the FWM in a gas-filled hollow fiber has been widely used for efficient frequency conversion via difference-frequency mixing [17, 18, 21, 23, 24], although no light amplification has been investigated to our knowledge. Use of the fundamental propagation modes is expected to lead to a broader phase-matching bandwidth than the regime based on high-order propagation modes. As both the amplified signal and the generated idler in the former have single-mode transverse beam profiles, output pulses are suitable for seeding the TW–PW OPCPA. More importantly, neither the amplification wavelength, nor wavelength dependence of the amplification gain, nor the phase-matching gas pressure for the FWOPA in this study are reproduced based simply by considering the linear phase mismatch for the FWOPA. The influence of the nonlinear phase mismatch from the cross-phase modulation (XPM) induced by the pump pulse needs to be taken into account in reproducing the amplified signal spectra. This contrasts with the account given in the previous report where only the linear phase mismatch was used to predict the phase-matching condition [22]. The FWOPA in a gas-filled hollow fiber reported here is hence in a different regime than that reported in the previous report.

This paper is organized as follows. First, wavelength and gas-pressure dependence of the phase mismatch and coherence length for the FWOPA in a gas-filled hollow fiber are discussed. It is shown that a broader amplification bandwidth is expected using the  $\text{EH}_{11}$  fundamental propagation mode rather than the high-order modes. Next, a set of coupled equations and an analytic model for the FWOPA are given as a basis to discuss experimental observations. Experimental observations on the FWOPA in a gas-filled hollow fiber with the  $\text{EH}_{11}$  propagation modes are then presented and discussed, especially in regard to the wavelength dependence of the amplification gain. Both the numerical simulation and the analytic model are used to

reproduce the experimentally measured spectrum of the amplified signal pulse. Finally, conclusions of this report are presented.

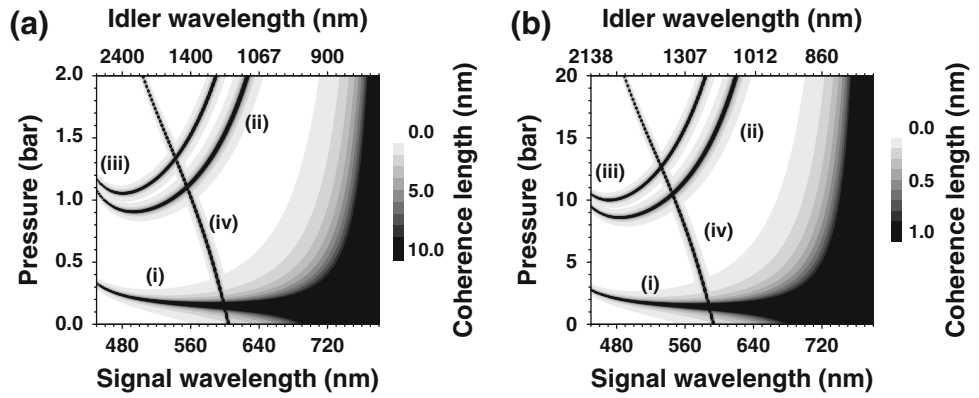
## 2 Theory

### 2.1 Phase mismatch

The propagation constant for a propagation mode inside a gas-filled hollow fiber  $\beta_k$  consists of two linear contributions. One relates to the gas medium filling the core ( $\beta_{k,m}$ ), and the other relates to the transverse propagation mode ( $\beta_{k,T}$ ). The propagation constant is given by  $\beta_k = (\beta_{k,m}^2 - \beta_{k,T}^2)^{1/2}$  [24, 25]. In a degenerate FWM, nonlinear polarization induced by the interaction of two radiation fields, namely the pump and signal fields with angular frequencies  $\omega_p$  and  $\omega_s$ , generates a frequency component at  $\omega_i$  (idler). Energy conservation forces the angular frequency of the idler to satisfy relation  $\omega_i = 2\omega_p - \omega_s$ . The linear phase mismatch  $\Delta\beta$  for this process is expressed as  $\Delta\beta = \beta_s + \beta_i - 2\beta_p$ , where  $\beta_p$ ,  $\beta_s$ , and  $\beta_i$  stand for the (linear) propagation constants of pump, signal, and idler fields, respectively. Light amplification via the FWOPA occurs in a wavelength range where the phase mismatch is small or the coherence length  $\pi/|\Delta\beta|$  is large.

The wavelength and gas-pressure dependence for the coherence length are calculated for two cases of the FWOPA with a gas-filled hollow fiber (Fig. 1). Ar gas is assumed to fill the core of the hollow fiber. In Fig. 1a, a core diameter for the hollow fiber of 450  $\mu\text{m}$  and a pump wavelength of 800 nm are assumed [22], whereas in Fig. 1b, a core diameter of 140  $\mu\text{m}$  and a pump wavelength of 784 nm are assumed. In both cases, several combinations of propagation modes are considered. When pump, signal, and idler pulses all propagate in mode  $\text{EH}_{11}$ , the phase-matching condition ( $\Delta\beta = 0$ ) is satisfied or the coherence length is large at a gas pressure [(i) in Fig. 1] much less than that for high-order propagation modes [(ii), (iii), and (iv) in Fig. 1]. This leads to a lower efficiency in the FWOPA compared with that for high-order propagation modes. The lower efficiency can be compensated using a narrower hollow fiber giving a higher phase-matching pressure and higher intensities of input pulses. For a core diameter of 450  $\mu\text{m}$ , the phase-matching pressure is less than 0.3 bar [(i) in Fig. 1a], whereas for a core diameter of 140  $\mu\text{m}$ , it is between 1 and 3 bar [(i) in Fig. 1b]. Compared with high-order propagation modes, use of only the  $\text{EH}_{11}$  mode leads to broadband phase matching as is expected from the data given in Fig. 1. FWOPA using a hollow fiber with a core diameter of 140  $\mu\text{m}$  and  $\text{EH}_{11}$  modes [(i) in Fig. 1b] was investigated in this study.

**Fig. 1** Wavelength and pressure dependence of coherence length for the FWOPA. For parameter settings, refer to main text. In both panels, coherence lengths are calculated for several combinations of propagation modes (pump, signal, and idler) of (i) (EH<sub>11</sub>, EH<sub>11</sub>, EH<sub>11</sub>), (ii) (EH<sub>11</sub>, EH<sub>11</sub>, EH<sub>21</sub>), (iii) (EH<sub>11</sub>, EH<sub>21</sub>, EH<sub>21</sub>), (iv) (EH<sub>32</sub>, EH<sub>22</sub>, EH<sub>32</sub>)



2.2 Amplification gain

Denoting the electric fields of the signal, idler, and pump pulses as  $\epsilon_s$ ,  $\epsilon_i$ , and  $\epsilon_p$ , respectively, the nonlinear interaction related to the FWOPA is expressed by the following coupled equations [26]:

$$\begin{aligned} \partial \epsilon_s / \partial z &= i D_s \epsilon_s \\ &+ i(\omega_s n_2 / c) T_s \left\{ 2 |\epsilon_p|^2 \epsilon_s + \epsilon_p^2 \epsilon_i^* \exp(-i \Delta \beta z) \right\}, \end{aligned} \tag{1}$$

$$\begin{aligned} \partial \epsilon_i / \partial z &= i D_i \epsilon_i \\ &+ i(\omega_i n_2 / c) T_i \left\{ 2 |\epsilon_p|^2 \epsilon_i + \epsilon_p^2 \epsilon_s^* \exp(-i \Delta \beta z) \right\}, \end{aligned} \tag{2}$$

$$\begin{aligned} \partial \epsilon_p / \partial z &= i D_p \epsilon_p \\ &+ i(\omega_p n_2 / c) T_p \left\{ |\epsilon_p|^2 \epsilon_p + 2 \epsilon_p^* \epsilon_i \epsilon_s \exp(i \Delta \beta z) \right\}, \end{aligned} \tag{3}$$

$$\begin{aligned} D_k &= -\alpha_k / 2 - (1/v_k - 1/v_s)(\partial / \partial t) - i(\beta_k^{(2)} / 2)(\partial^2 / \partial t^2) \\ &+ i(\beta_k^{(3)} / 6)(\partial^3 / \partial t^3) + \dots, \end{aligned} \tag{4}$$

where  $n_2$  stands for the nonlinear refractive index of the medium, which for a gas medium is proportional to the gas pressure;  $T_k$  contains a contribution from self-steepening, specifically,  $T_k = \{1 + (i/\omega_k)(\partial/\partial t)\}$  with  $\alpha_k$  the linear propagation loss and  $v_k$  the group velocity of each field.  $\beta_k^{(2)}$  and  $\beta_k^{(3)}$ , respectively, are the group-delay dispersion (GDD) and the third-order dispersion (TOD). Subscripts  $s$ ,  $i$ , and  $p$  refer to signal, idler, and pump, respectively. Intensities of the amplified signal pulse and idler pulse are assumed to be low, and the nonlinear phase shift arising from the self-phase modulation (SPM) induced by signal and idler pulses is neglected. Similarly, efficiency in the XPM induced by the signal and idler pulses is assumed to be negligibly small; these conditions are met in this study. The SPM induced in the pump pulse and the XPM induced in the signal and idler pulses arising from the intense pump pulse are included in the equations.

By assuming no pump depletion, no self-steepening effect, negligibly small effects from GDD, TOD, and linear propagation losses, analytical solutions of the resulting coupled equations are found that qualitatively determine the effect of nonlinear phase modulation on the FWOPA. The modified coupled equations are as follows:

$$\partial \epsilon_s / \partial z = i(\omega_s n_2 / c) \left\{ 2 |\epsilon_p|^2 \epsilon_s + \epsilon_p^2 \epsilon_i^* \exp(-i \Delta \beta z) \right\}, \tag{5}$$

$$\partial \epsilon_i / \partial z = i(\omega_i n_2 / c) \left\{ 2 |\epsilon_p|^2 \epsilon_i + \epsilon_p^2 \epsilon_s^* \exp(-i \Delta \beta z) \right\}, \tag{6}$$

$$\epsilon_p(z) = \epsilon_p(0) \exp \left\{ i(\omega_p n_2 / c) |\epsilon_p(0)|^2 z \right\}, \tag{7}$$

where  $\epsilon_p(0)$  is the electric field of the input pump pulse at  $z = 0$ . The analytical solution of the coupled equations (Eqs. 5–7) is as follows:

$$\epsilon_s(z) = \{ \cosh(gz) - i(\kappa/2g) \sinh(gz) \} \epsilon_s(0) \exp\{i\Phi\}, \tag{8}$$

$$\Phi = \left\{ -\kappa/2 + 2(n_2/c)\omega_s |\epsilon_p|^2 \right\} z \tag{9}$$

$$\kappa = \Delta\beta + \Delta\beta_{NL}, \tag{10}$$

$$g = \left\{ (n_2 |\epsilon_p|^2 / c)^2 (\omega_p^2 - \Delta\omega^2) - (\kappa/2)^2 \right\}^{1/2} \tag{11}$$

In the above, the effective phase mismatch  $\kappa$  consists of two contributions: the linear phase mismatch ( $\Delta\beta$ ) and a nonlinear contribution  $\Delta\beta_{NL} = 2(n_2/c)|\epsilon_p|^2\omega_p$ , which depends on the pump intensity and is hereafter termed the nonlinear phase mismatch. The nonlinear phase mismatch results from the XPM induced in the signal and idler pulses. In obtaining Eqs. 10 and 11, the relation  $\omega_s - \omega_p = \omega_p - \omega_i = \Delta\omega$  was used. The amplification gain ( $G$ ) is then defined as  $|\epsilon_s(z)|^2/|\epsilon_s(0)|^2$ , giving the following expression:

$$G = \cosh^2(gz) + (\kappa/2g)^2 \sinh^2(gz) \tag{12}$$

When the same derivation is repeated after dropping the terms related to the SPM and XPM in Eqs. 5–7, the same expression, Eq. 12, is obtained for the amplification

gain, but with  $\kappa = \Delta\beta$ . This solution gives the amplification gain expected when the XPM does not affect the amplification process. These solutions are used below when discussing nonlinear phase modulation effects on the experimentally observed wavelength dependence of amplification gain.

### 3 Experiment

An experimental setup schematically shown in Fig. 2 was used for investigating the FWOPA in a gas-filled hollow fiber seeded with a supercontinuum pulse. A small fraction ( $<5 \mu\text{J}$ ) of the laser pulse from a Ti:sapphire regenerative amplifier (1 kHz, 1 mJ/pulse, 100 fs, 784 nm, Concerto, Thales) was focused onto a 3-mm-thick sapphire plate to generate a supercontinuum. The generated continuum (hereafter termed the seed pulse) and the remaining part of the near-infrared pulse (hereafter termed the pump pulse) were then spatially and temporally overlapped after the pump pulse passed through an optical delay line. For spatial overlap, a short-pass filter (3-mm-thick fused-silica substrate, NT64-332, Edmund Optics) was used that transmitted wavelength components shorter than 700 nm at an angle of incidence of  $45^\circ$ . The two pulses were focused with a concave mirror (a focal length of 500 mm) into an Ar-filled hollow fiber made of fused silica (a length of 500 mm, a core diameter of  $140 \mu\text{m}$ , an Ar pressure of 0.9 bar). The hollow fiber was placed on a V-groove put inside a vacuum chamber equipped with 0.5-mm-thick fused-silica windows. After collimation using a concave mirror, the output pulses were passed twice through a high reflector removing the pump wavelength component. The spectrum of the transmitted seed pulse was measured by focusing it with a concave mirror into an optical fiber coupled to a multi-channel spectrometer (USB2000, Ocean Optics).

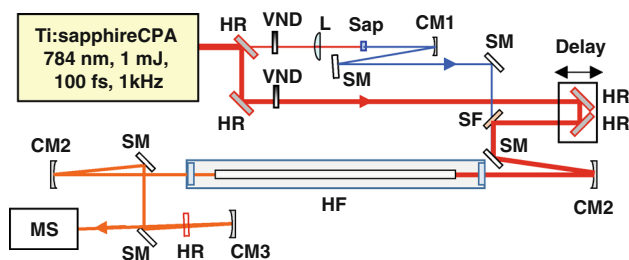


**Fig. 2** Experimental setup. HR high reflector at 784 nm; VND variable neutral-density filter; L plano-convex lens ( $f = 60 \text{ mm}$ ), Sap sapphire plate, SF short-pass filter, HF hollow fiber chamber, CM1-3, concave mirrors,  $f = 100 \text{ mm}$  (CM1),  $500 \text{ mm}$  (CM2),  $200 \text{ mm}$  (CM3); SM silver mirrors, MS multi-channel spectrometer

### 4 Results

The energy of the input pump pulse was  $470 \mu\text{J}$  in front of the entrance window of the chamber whereas that of the output pump pulse was  $220 \mu\text{J}$ . In other words, the energy throughput of the hollow fiber chamber was 47 %. Given the  $\text{EH}_{11}$  propagation modes, the energy throughput in the hollow fiber itself is predicted to be 68 % when assuming perfect coupling between input pump pulse and  $\text{EH}_{11}$  mode [25]. Fresnel losses on the chamber windows reduce this value to 59 %. The difference between the experimental throughput of 47 % and the theoretical value of 59 % arises from the imperfect coupling of the input pulse into the hollow fiber in the setup. Evacuating the gas chamber did not change the output energy, indicating negligible nonlinear loss from multi-photon ionization and self-focusing, and no detectable change in the propagation modes inside the hollow fiber by the presence of the Ar gas.

The spectra of the output seed from the gas-filled hollow fiber are shown in Fig. 3; there, the input seed spectrum extends from 450 to 700 nm. The longest wavelength of the seed pulse was determined by the cutoff wavelength of the short-pass filter (SF in Fig. 2) and the high reflector after the hollow fiber. When only the pump pulse was focused into the hollow fiber, no spectral component was detected in the seed wavelength range (Fig. 3). When both the input pump and seed pulses were used simultaneously, the peak intensity of the seed pulse increased 300 times. When the hollow fiber chamber was evacuated, no spectral change was observed by the presence of the pump pulse. These observations suggest that the FWOPA process in the Ar-filled hollow fiber induces increases in seed intensity.

The input seed pulse was positively chirped when focused into the hollow fiber and was longer than the pump

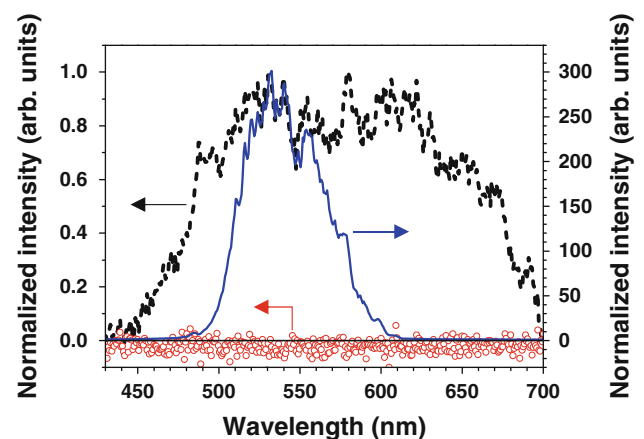


**Fig. 3** Output seed spectra obtained when only the seed pulse (broken line, left ordinate), only the pump pulse (open circle, left ordinate), and both the seed and pump pulses (solid line, right ordinate) were focused into the hollow fiber. All spectra are normalized by the peak intensity for the seed-pulse-only spectrum

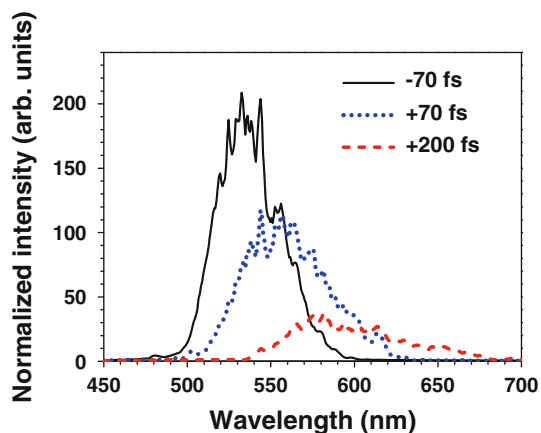


**Fig. 4** Amplified seed spectra at time delays of  $-70$  (solid),  $+70$  (dotted), and  $+200$  fs (broken line). Each spectrum is normalized by the peak intensity of the seed-pulse-only spectrum

pulse. This arose mainly from the GVD induced in the seed pulse when it propagated through the sapphire plate to generate the supercontinuum and the glass substrate of the dichroic mirror to spatially combine the input pump and seed pulses. The change in the amplified wavelength component in the signal pulse that occurred while changing the time delay of the pump pulse gives an estimate for the GDD in the signal pulse around 550 nm of about  $1,000 \text{ fs}^2$ . The broader pulse duration of the signal pulse than the pump pulse has led to a narrower spectrum for the amplified seed pulse compared with the input seed pulse (Fig. 3). The amplified spectrum extends from 470 to 610 nm, whereas the input seed spectrum extends from 450 to 700 nm, because only a limited wavelength component from 470 to 610 nm in the seed pulse temporally overlaps with the shorter pump pulse. The full width at half maximum of the amplified spectrum supports a transform-limited pulse duration of 7.4 fs when assuming a Gaussian pulse shape. By integrating the spectral intensities of the amplified seed in this wavelength range and dividing it by the corresponding integrated spectrum of the unamplified seed pulse, the gain in the wavelength range can be estimated at 150. When the same estimation was repeated in the full

wavelength range of the seed pulse (450–700 nm), which is hereafter denoted as the amplification gain, the result was 100. The energy of the amplified seed pulse was 46 nJ as measured with a silicon-based optical sensor (OP-2 VIS, Coherent Inc.). The amplification gain of 100 is similar to those reported for the FWOPA in bulk media [15].

Because of the frequency chirp in the seed pulse, the amplification wavelength shifted with the change in the time delay of the pump pulse. This was used to investigate the wavelength range in which the seed pulse was parametrically amplified. The amplification was observed in a wavelength range of 500–700 nm ( $5,700 \text{ cm}^{-1}$ ). Shown in Fig. 4 are three typical spectra of the amplified seed measured at three different time delays of  $\pm 70$  and  $+200$  fs at a constant gas pressure of 0.8 bar; the origin for the time delay is defined as the time delay in the above experiment. The center wavelengths of the amplified spectra were 535 ( $-70$  fs), 555 ( $+70$  fs), and 590 nm ( $+200$  fs). The maximum amplification gain was obtained at around 535 nm.

The pressure dependence of the amplification gain at the three time delays was investigated (Fig. 5a). In all cases, the amplification gain peaked at around 0.8–0.9 bar. The peak gain is much higher at the time delay of  $-70$  fs (center wavelength of 535 nm) than the other time delays of  $+70$  fs (center wavelength of 555 nm) and  $+200$  fs (center wavelength of 590 nm), indicating that the wavelength dependence of the amplification gain is inhomogeneous. This inhomogeneity is also indicated in the result in Fig. 4. When the same measurement was repeated after reducing the input pump energy to  $150 \mu\text{J}$ , the peak gas pressures changed to 1.3–1.4 bar (Fig. 5b), which are higher than those in the above measurement. Moreover, inhomogeneity in the wavelength dependence of the amplification gain was not seen in this case (see Fig. 5b).

## 5 Discussion

To discuss the source of the inhomogeneity in the wavelength dependence of the amplification gain, an input pump

**Fig. 5** Energy gain with respect to gas pressure obtained for **a** intense ( $470 \mu\text{J}$ ) and **b** relatively weak ( $150 \mu\text{J}$ ) pump pulses. In each figure, the amplification gains obtained for the three pump time delays of  $-70$ ,  $+70$ , and  $+200$  fs are marked with *squares*, *circles*, and *triangles*, respectively

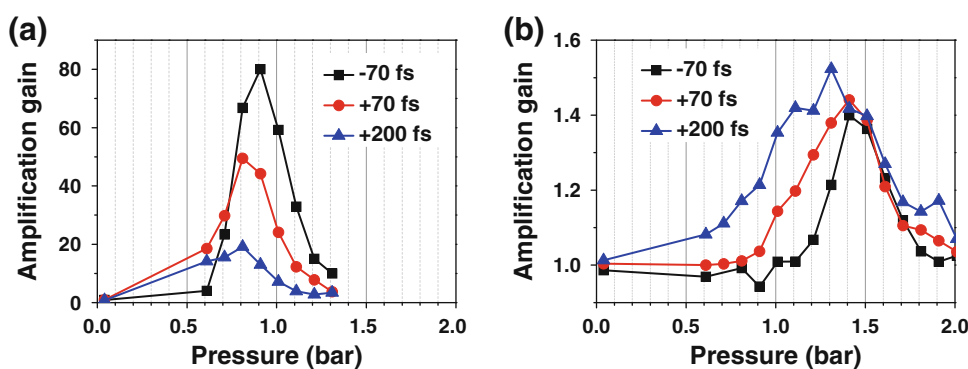


**Fig. 6** Spectra of the output pump pulses measured at gas pressures 0.61, 0.81, 1.0, and 1.2 bar. Experimental spectra are indicated with *dotted lines*, whereas those from numerical simulations are marked by *solid line*

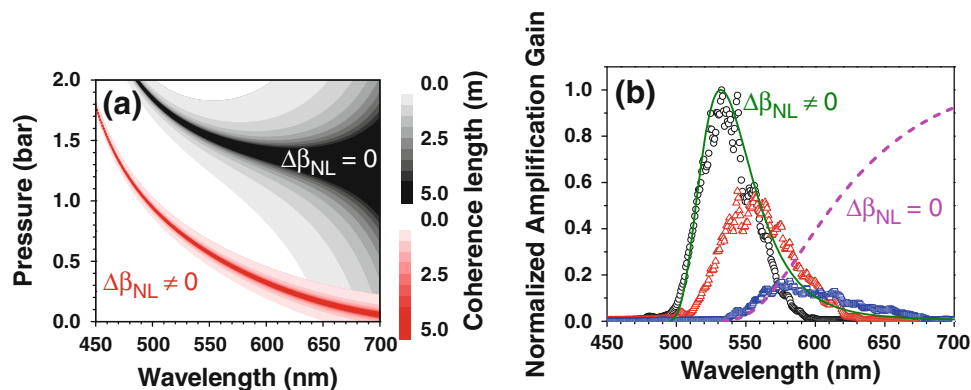
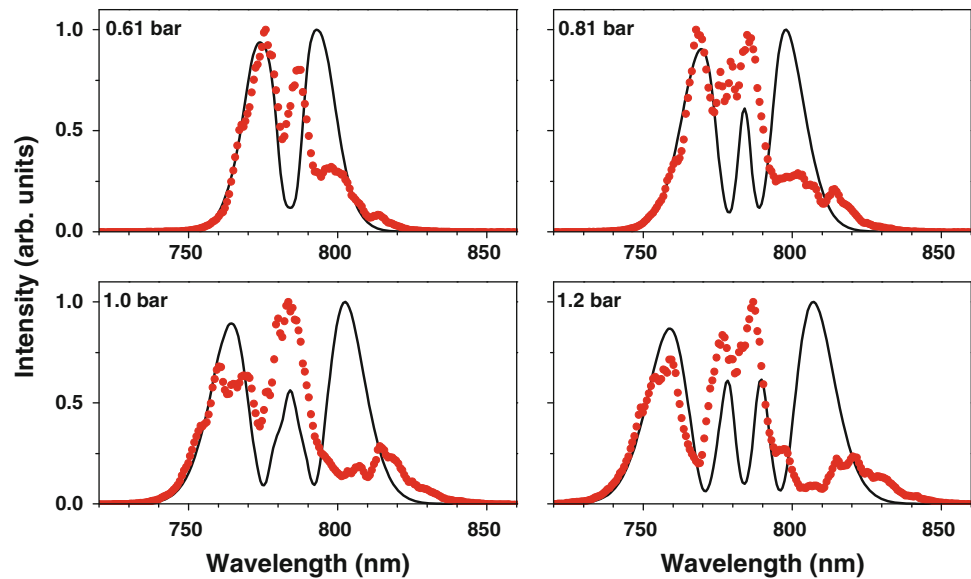


**Fig. 7** **a** The coherence length as a function of seed wavelength and pressure with nonlinear phase mismatch (*red*  $\Delta\beta_{NL} \neq 0$ ) and without (*black*  $\Delta\beta_{NL} = 0$ ). **b** Normalized amplification gain with respect to seed wavelength calculated using Eq. 12 for  $\Delta\beta_{NL} \neq 0$  (*solid line*)

and  $\Delta\beta_{NL} = 0$  (*broken line*). For comparison, experimental data given in Fig. 5 are also reproduced with *open circles* ( $-70$  fs), *triangles* ( $+70$  fs), and *squares* ( $+200$  fs); data are normalized by the peak of the  $-70$ -fs curve (*open circles*)

peak intensity of  $27 \text{ TW/cm}^2$  is assumed. This assumption is based on the parameter values for the pump pulse duration of 150 fs, a beam radius of  $51 \mu\text{m}$  for the  $\text{EH}_{11}$  mode inside the hollow-core fiber, and the pump pulse energy used in the experiment (Figs. 3, 4, 5). These parameters reproduce the experimentally measured spectra of the output pump pulses (Fig. 6), where Eqs. 3 and 4 were solved numerically by the split-step Fourier method [27]. By considering the linear propagation loss for the  $\text{EH}_{11}$  mode, the pump intensity is  $18 \text{ TW/cm}^2$  at the exit of the hollow fiber. Using this value for the pump intensity, the dependence of the coherence length with respect to the signal wavelength and the gas pressure was calculated (Fig. 7a), in which Eq. 10 was used to calculate the effective phase mismatch ( $\kappa = \Delta\beta + \Delta\beta_{NL}$ ). This mismatch was then used for calculating the coherence length as  $\pi/|\kappa|$ . The coherence length calculated considering only the linear phase mismatch ( $\kappa = \Delta\beta$ ) is also shown in the same figure.

The calculated pressure dependence of the coherence length agrees with the experimental observation when both linear and nonlinear phase mismatch are taken into account. The coherence length peaks at around 530 nm for a gas pressure of 0.8 bar, which is consistent with the experimentally measured peak pressure of the amplification gain of around 0.8 bar (Fig. 5a). Neglecting the nonlinear phase mismatch and considering only the linear phase mismatch, the calculated coherence length peaks at around 1.6 bar for a signal wavelength of 530 nm, which fails to agree with the experimental observation. The curve calculated for  $\kappa = \Delta\beta + \Delta\beta_{NL}$  predicts that the phase-matching pressure is high for short signal wavelengths, which should result in a high peak amplification gain. This is also consistent with the experimental observation (Fig. 5a), in which the peak amplification gain is higher for the short signal wavelength (time delay of  $-70$  fs) than the other two cases.

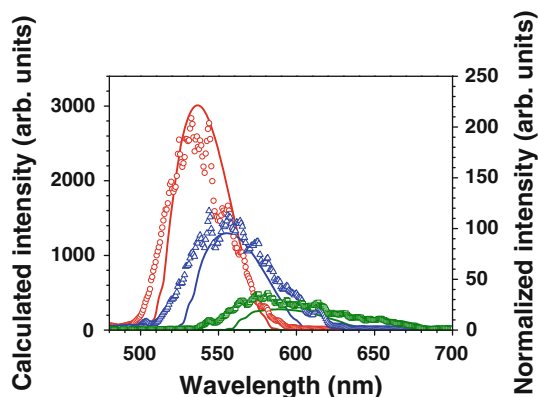


**Fig. 8** Amplification gain simulated using the coupled equations (*left ordinate, solid lines*). Experimental spectra from Fig. 5 are also shown for comparison (*right ordinate: the time delay of  $-70$  fs, open circle;  $+70$  fs, triangle,  $+200$  fs, square*)

For a low-intensity pump pulse, the influence of the XPM is not large and the amplification gain is expected to peak at a pressure around 1.6 bar. This is consistent with the measured peak pressure around 1.4–1.5 bar when the low-energy pump pulse was used (Fig. 5b). The two-dimensional plot of the coherence length ( $\Delta\beta_{\text{NL}} = 0$ , Fig. 7a) indicates that the wavelength dependence of the peak pressure of the coherence length is small in the wavelength range of 530–590 nm when the nonlinear phase mismatch is negligibly small. This leads to a small wavelength dependence of the amplification gain, which is consistent with a small inhomogeneity in the observed wavelength dependence of the peak amplification gain under a low pump intensity (Fig. 5b).

The wavelength dependence of the amplification gain is calculated using the analytical solution of the amplification gain, Eq. 12. When considering both linear and nonlinear phase mismatches, the calculation reproduces well the relative peak intensities of the amplified seed spectra measured at the three different pump time delays (Fig. 7b). In contrast, when the calculation was repeated after neglecting the nonlinear phase mismatch, the calculated wavelength dependence of the amplification gain did not agree with the experimental observation (Fig. 7b). The spectral shape of each amplified signal pulse is well reproduced with numerical simulations based on the coupled equations (Eqs. 1–4) solved with the split-step Fourier method [27]. Here, the input seed pulse is assumed to have a super-Gaussian spectral shape with a full width at half maximum of 180 THz, in accordance with the experimental spectrum extending from 450 to 700 nm. The linear frequency chirp with a GDD of  $1,000 \text{ fs}^2$  is assumed, as estimated from the experimentally measured relative group delays of the wavelength components of 535, 550, and 590 nm. Calculated spectral features (Fig. 8) are in fair agreement with the

experimental spectra. The relative intensities of the three amplified signal pulse are well reproduced by the numerical simulation. The difference in the absolute values of the spectral intensities between the experiment and the simulation might be related to the imperfect spatial overlap between the pump and signal modes in the experiment.

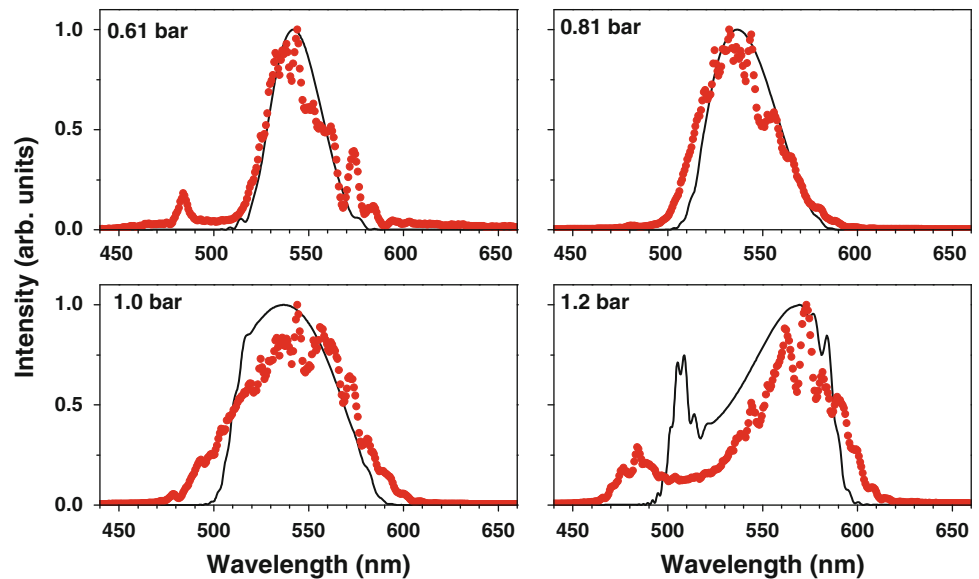
From these investigations, the nonlinear phase mismatch does appreciably affect the amplification wavelength, the wavelength dependence of the amplification gain, and the phase-matching pressure for the FWOPA. Consideration of only the linear phase mismatch fails to reproduce these. From analysis using the analytical solution (Eqs. 10–12), these results are not related to the pulse duration of the pump pulse. Hence, the above discussion should apply also to long pump pulses, e.g., of a picosecond duration, provided that the pump intensity is sufficiently high to induce a nonlinear refractive index change.

In the presence of SPM and XPM induced by the pump pulse, an amplified signal pulse is spectrally broadened during amplification. However, the efficiency in the nonlinear phase modulations obtained in this study is not as large as those in a previous study [22]; slight spectral broadening of the amplified signal pulse has been observed. The spectral width of the amplified signal pulse increased with increasing gas pressure (Fig. 9). The spectrum of the amplified signal pulse was simulated numerically using Eqs. 1–4, the result of which is given in the same figure. Although there is a slight difference in the spectral width between the experimental spectrum and the simulated spectrum, the spectral shape of the simulated curves qualitatively agrees with the experimental spectrum.

## 6 Conclusions

In conclusion, the FWOPA in a gas-filled hollow fiber was investigated for direct amplification of a supercontinuum pulse. The fundamental propagation mode  $\text{EH}_{11}$  was used as the propagation mode for the pump, signal, and idler pulses. Amplification in the wavelength range 500–700 nm and an amplification gain up to 100 were obtained when pumping at 784 nm. The amplification bandwidth supports sub-10-fs pulse durations. For the FWOPA with a high amplification gain, the influence of the nonlinear phase mismatch arising from the XPM induced by the intense pump pulse needed to be taken into account. The nonlinear phase mismatch lowers the phase-matching pressure and substantially modifies the wavelength dependence of the amplification gain and amplification bandwidth. If the nonlinear phase modulation is not considered, the phase-matching pressure and the wavelength dependence of the amplification gain are not reproduced; this conclusion contrasts a previous study based on high-order propagation

**Fig. 9** Spectra of the output signal pulses for gas pressures of 0.61, 0.81, 1.0, and 1.2 bar. Experimental spectra are marked with *dotted lines*, whereas those obtained by numerical simulations with *solid lines*



modes and narrowband input seed pulses [22]. To obtain a broader bandwidth after the amplification, use of a short pump pulse (about 200 fs or shorter) with a higher intensity than that used in this study might be useful in yielding simultaneous amplification and spectral broadening using XPM. By combining the technique reported herein and the high-power picosecond or sub-picosecond laser technologies in developing a preamplifier for the Ti:sapphire-free TW-PW OPCPA, the nonlinear pulse compression technique might be a key technique providing 200-fs or shorter pump pulses at 515 nm [28].

**Acknowledgments** This work was supported by Kyushu University Interdisciplinary Programs in Education and Projects in Research Development.

## References

1. A. Baltuška, T. Fuji, T. Kobayashi, *Opt. Lett.* **27**, 306 (2002)
2. D. Brida, G. Cirrmi, C. Manzoni, S. Bonora, P. Villorosi, S. De Silvestri, G. Cerullo, *Opt. Lett.* **33**, 741 (2008)
3. Z. Major, S.A. Trushin, I. Ahmad, M. Siebold, C. Wandt, S. Klingebiel, T.-J. Wang, J.A. Fülöp, A. Henig, S. Kruber, R. Weingartner, A. Popp, J. Osterhoff, R. Hörlein, J. Hein, V. Pervak, A. Apolonski, F. Krausz, S. Karsch, *Rev. Laser Eng.* **37**, 431 (2009)
4. S. Witte, R.T. Zinkstok, A.L. Wolf, W. Hogervorst, W. Ubachs, K.S.E. Eikema, *Opt. Express* **14**, 8168 (2006)
5. D. Herrmann, L. Veisz, R. Tautz, F. Tavella, K. Schmid, V. Pervak, F. Krausz, *Opt. Lett.* **34**, 2459 (2009)
6. K. Schmid, L. Veisz, F. Tavella, S. Benavides, R. Tautz, D. Herrmann, A. Buck, B. Hidding, A. Marcinkevicius, U. Schramm, M. Geissler, J. Meyer-ter-Vehn, D. Habs, F. Krausz, *Phys. Rev. Lett.* **102**, 124801 (2009)
7. Y. Deng, A. Schwarz, H. Fattahi, M. Ueffing, X. Gu, M. Ossiander, T. Metzger, V. Pervak, H. Ishizuki, T. Taira, T. Kobayashi, G. Marcus, F. Krausz, R. Kienberger, N. Karpowicz, *Opt. Lett.* **37**, 4973 (2012)
8. M. Schulz, R. Riedel, A. Willner, T. Mans, C. Schnitzler, P. Russbuehldt, J. Dolkemeyer, E. Seise, T. Gottschall, S. Hädrich, S. Duesterer, H. Schlarb, J. Feldhaus, J. Limpert, B. Faatz, A. Tünnermann, J. Rossbach, M. Drescher, F. Tavella, *Opt. Lett.* **36**, 2456 (2011)
9. C. Homann, M. Bradler, M. Förster, P. Hommelhoff, E. Riedle, *Opt. Lett.* **37**, 1673 (2012)
10. R. Antipenkov, A. Varanavičius, A. Zaukevičius, A.P. Piskarskas, *Opt. Express* **19**, 3519 (2011)
11. F. Tavella, A. Marcinkevicius, F. Krausz, *New J. Phys.* **8**, 219 (2006)
12. H. Valtna, G. Tamosauskas, A. Dubietis, A. Piskarskas, *Opt. Lett.* **33**, 971 (2008)
13. A. Dubietis, G. Tamošauskas, P. Polesana, G. Valiulis, H. Valtna, D. Faccio, P. Di Trapani, A. Piskarskas, *Opt. Express* **15**, 11126 (2007)
14. A. Penzkofer, H.J. Lehmeier, *Opt. Quantum Electron.* **25**, 815 (1993)
15. A. Dubietis, G. Tamošauskas, G. Valiulis, A. Piskarskas, *Laser Chem.* **2008**, 1 (2008)
16. J. Liu, Y. Kida, T. Teramoto, T. Kobayashi, *Opt. Express* **18**, 2495 (2010)
17. C.G. Durfee, S. Backus, H.C. Kapteyn, M.M. Murnane, *Opt. Lett.* **24**, 697 (1999)
18. A.E. Jailaubekov, S.E. Bradforth, *Appl. Phys. Lett.* **87**, 021107 (2005)
19. F. Théberge, N. Aközbek, W. Liu, A. Becker, S. Chin, *Phys. Rev. Lett.* **97**, 023904 (2006)
20. T. Fuji, T. Horio, T. Suzuki, *Opt. Lett.* **32**, 2481 (2007)
21. Y. Kida, J. Liu, T. Teramoto, T. Kobayashi, *Opt. Lett.* **35**, 1807 (2010)
22. D. Faccio, A. Grün, P.K. Bates, O. Chalus, J. Biegert, *Opt. Lett.* **34**, 2918 (2009)
23. C.G. Durfee, S. Backus, M.M. Murnane, H.C. Kapteyn, *Opt. Lett.* **22**, 1565 (1997)
24. C.G. Durfee, L. Misoguti, S. Backus, H.C. Kapteyn, M.M. Murnane, *J. Opt. Soc. Am. B* **19**, 822 (2002)
25. E.A.J. Marcatili, R.A. Schmeltzer, *Bell Syst. Tech. J.* **43**, 1783 (1964)
26. Y. Kida, T. Kobayashi, *J. Opt. Soc. Am. B* **28**, 139 (2010)
27. G.P. Agrawal, *Nonlinear fiber optics* (Academic, San Diego, 2006)
28. A. Dubietis, G. Valiulis, R. Danielius, A. Piskarskas, *Pure Appl. Opt.* **7**, 271 (1998)